https://doi.org/10.20965/jdr.2022.p0670

Paper:

A Half-Year Long Observation at Sakurajima Volcano, Japan Using a Multi-Channeled Seismometer System with Phase-Shifted Optical Interferometry

Haruhisa Nakamichi*,†, Yoshiharu Hirayama, Toshiharu Ikeda**, Hiroshi Ando**, and Keiji Takeuchi****

*Sakurajima Volcano Research Center, Disaster Prevention Research Institute, Kyoto University
1722-19 Sakurajima-Yokoyama-cho, Kagoshima, Kagoshima 891-1419, Japan
†Corresponding author, E-mail: nakamiti@svo.dpri.kyoto-u.ac.jp
**Hakusan Corporation, Fuchu, Japan
[Received December 10, 2021; accepted June 16, 2022]

The performance of a multi-channel seismometer system with phase-shifted optical interferometry was improved by newly introduced sensors and a processing unit. The current version of the system consists of three optical wired seismometers and the unit. We deployed the system at Sakurajima Volcano and successfully operated it from June to December 2019. As the Sakurajima Volcano frequently erupts, a number of eruption events were observed during the observation period, as were a number of lightning strikes. In this study, we evaluated the observation performance of the volcanic earthquake and the noise caused by the lightning, using the spectrum and amplitude of the waveform. The results show that this sensor can observe earthquakes caused by eruptions as well as ordinary seismometers do. When the lightning struck, pulsed noise with power in a wide frequency band was observed in the existing seismometer, but not in the new sensor. Therefore, the observation was not affected by lightning. In addition, this system was found to be effective in the array analysis of volcanic earthquakes.

Keywords: seismic observation, optical interferometry, volcano observatory, eruption, lightning

1. Introduction

Because of the high density of human population and economic activity in Japan, permanent seismic observations have been carried out by installing borehole stations to ensure a sufficiently high signal-to-noise (S/N) ratio when observing micro-earthquakes [1–4]. This effort has also been made for volcanoes. Borehole seismometers at depths of several hundred meters have been installed at major active volcanoes in Japan, and continuous observations have been carried out [5], in which electricity is supplied from the ground to the subsurface sensor, the voltage output from the subsurface sensor is received on the ground, and digital-to-analog conversion is performed. Borehole seismic observations are thus affected by lightning because the electric wire is drawn from the ground to the subsurface sensor, and in some cases, the sensor may be damaged by lightning. In the case of failure of a borehole sensor, it is necessary to replace the sensor; however, this is expensive and time consuming. Moreover, seismometers are installed on the surface of the ground around the volcanic crater; however, they are often damaged by lightning due to the high altitude and lack of obstructions. Therefore, the construction of an observation system that is not affected by lightning because there are no electric or electronic parts of the sensors is desirable for observations with a stable high S/N ratio in the volcano.

A distributed acoustic sensing (DAS) system is a seismic observation system that uses optical fibers as a seismic sensor and does not have electrical and electronic components in the sensor [6]. In recent years, DASs have been applied in geophysical and volcanological researches [7]. DAS measures the back-scattering of a laser beam irradiated in the optical fiber and observes the strain in the extension direction of the optical fiber. DAS can conduct high-density seismic observations at locations where an optical fiber is installed; however, it cannot measure 3D displacement or acceleration at those locations. In addition, because the dynamic range is narrow, approximately 60 dB, the S/N ratio is not sufficiently high. Therefore, it is necessary to improve the S/N ratio by stacking seismic data from source locations that are close to each other.

Recently, a seismic observation system using optical interferometry has been developed [8, 9]. Similar to a DAS, this system uses an optical fiber. However, optical fibers are used not as seismic sensors but as signal communication channels. The seismic sensor consists of only an optical fiber and mechanical parts and does not require a power supply, and the dynamic range of the seismic sensor is as large as 120 dB [8, 9]. In principle, many sensors can be connected to a single pair of optical fibers

Table 1. Specifications of the newly developed and JOGMEC Phase 1 systems.

System	Fiber	Sensor							
	Type	Components	Frequency range [Hz]	Dynamic range [dB]	Measurement range [G]	Natural frequency [Hz]	Damping factor	Size [cm]	Weight [kg]
This study	Single-mode (general purpose)	3	0.1–20	130	±1.2	23.1	0.68	12 × 15 × 9	3
JOGMEC Phase 1	Polarization maintaining	3	0.1–50	120	±4.0	52.2	0.60	20 × 20 × 20	7

so that a multi-channel system can be constructed for a seismic array. The maximum number of channels is 33 for the current optical interferometry sensor system under reasonable conditions. An optical interferometry sensor system was used to observe the Asama and Sakurajima volcanoes in Japan, and it was confirmed that volcanic earthquakes and tremors could be observed without being inferior to existing seismometers [10]. However, owing to the short duration of these observations, no evaluation of long-term stability has been performed, and because the observations were not conducted during a period that includes the typhoon and rainy seasons, the effects of lightning strikes were not assessed. In addition, the observation of earthquakes caused by volcanic eruptions was insufficient owing to their short duration.

In the new system, the sensor part was downsized and the natural frequency was changed to a lower frequency than in the previous system [10]. This study compares the newly developed optical interferometry sensor system with the previous system and describes the observation of Sakurajima Volcano using the new system for six months from June 2019. We also describe the results of the analysis of volcanic earthquakes observed during the observation period, especially those associated with volcanic eruptions, and the effect of lightning strikes on seismic waveforms. During this period, many volcanic eruptions occurred in Sakurajima, and sufficient data were obtained to evaluate the observation performance of volcanic earthquakes and the impact of lightning strikes. The results of the array analysis of earthquakes associated with volcanic eruptions will be provided, as array observations can be performed with the optical interferometry sensor system, which has three separate seismometers forming a triangle. Although this is a minimum configuration as a seismic array, if sufficient accuracy can be obtained for the array analysis by this configuration, the significance of carrying out larger-scale array observations with many more sensors in volcanoes becomes clear.

2. Newly Developed Phase-Shifted Optical Interferometry System

As the principle and equipment of the optical interferometry sensor system have been explained in detail in previous studies [8–10], the principle of vibration measurement in the optical interferometry sensor system is briefly described here. The optical interferometry sensor system has a vibration sensor part (i.e., seismometer) that consists of a spring, mass and damper adjustable for critical damping. When the housing of the sensor moves, the weight inside behaves as a fixed point because of inertia, and the relative displacement reflects ground motion. Optical interferometry can measure displacement very precisely. In the optical interferometry method, the phase difference between the reference light and measurement light is obtained from the signal level of the interference light when both lights interfere with each other. By delaying the measurement light appropriately, the interfering, reference, and measurement lights can be separated and the phase difference can be determined with high precision by directly measuring the signals. The phase difference is proportional to the relative displacement of the weight to the enclosure, and the displacement is proportional to the acceleration of the forced vibration in a frequency range lower than the natural frequency of the sensor; therefore, the vibration sensor can be regarded as an accelerometer.

Compared with the JOGMEC Phase 1 (JOG1) system [10] used in the Asama and Sakurajima volcanoes, the major improvements in this new optical interferometry sensor system are the reduction in the size and weight of the sensor part, lower natural frequency, and change from a polarization-maintaining optical fiber to a general-purpose optical fiber. The specifications of the fiber and sensor parts of the new optical interferometry sensor system and JOG1 system are listed in **Table 1**. Note that the optical transceiver, receiver, and signal processing units of the optical interferometry sensor system were not changed. Therefore, an AC power supply is necessary for the operation of the system. The maximum power consumption is 500 W, which is the same as that of the JOG1 system. The new compact and lightweight design allows for greater flexibility in seismometer installation, and the lower natural frequency allows for greater applicability to volcanic earthquake monitoring. However, the measurement amplitude range has been narrowed from ±4.0 G for the JOG1 system to ±1.2 G for this system (**Table 1**). However, the dynamic range was improved by 10 dB compared to the JOG1 system owing to the low noise of the optical interferometry sensor (**Table 1**). In addition, because a general-purpose optical fiber is used in the new system, a vacant fiber in the existing optical fiber bundle can be used for seismic obser-

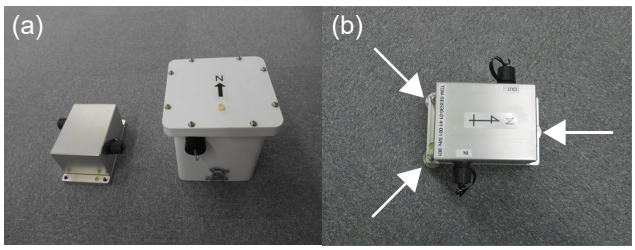

Fig. 1. (a) New 3-component sensor unit housing (left) and the JOGMEC Phase 1 sensor unit housing (right). (b) The new housing is supported at three points by adjustable feet (white arrows), and the leveling can be adjusted with a water leveler.

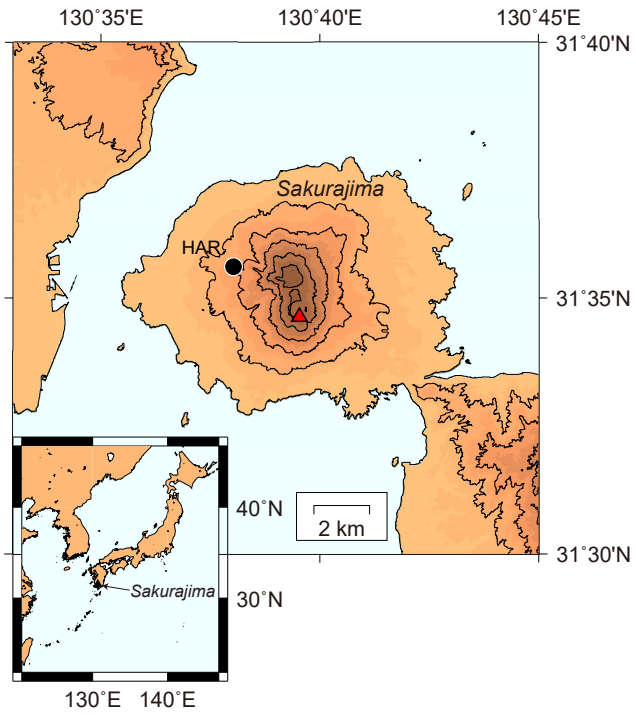

Fig. 2. Sakurajima Volcano and the location of the optical interferometry sensor system (black circle indicates the Harutayama Observatory, HAR). The red triangle shows the center of the volcanic eruption at Minamidake Crater.

vation by the new system. For the same length of optical fiber, the cost of a general-purpose fiber is one-thirtieth that of a polarization-maintaining optical fiber, which was used in the JOG1 system.

Figure 1 shows the new unit housing of the sensor and sensor unit housing of the JOG1 system. Both have one vertical component and two orthogonal horizontal components in each housing unit. The new housing is supported at three points by adjustable feet, and the leveling can be adjusted using a water leveler, unlike the JOG1 sensor, which does not have adjustable feet. The new sensor unit is compact and lightweight. Its volume is 20% of the volume of the housing of the JOG1 system, and the weight, including the seismometer, is 43% of the weight of the JOG1 housing (**Table 1**).

3. Experiment at Sakurajima Volcano in 2019

We carried out a seismic observation experiment using an optical interferometry sensor system with three 3-component sensors at the Harutayama Observatory (HAR), Kyoto University, from 16:00 (JST) on June 5, 2019, to 9:00 on December 5, 2019. The HAR is located at Sakurajima Volcano, where volcanic eruptions occur most frequently in Japan, and is situated approximately 2.7 km northwest of Minamidake, where the crater is located (**Fig. 2**). The aims of the experiments were 1) to evaluate the stability of the six-month operation, 2) to show the basic specifications from the comparison with the conventional seismometer, 3) to show the array analysis of volcanic earthquakes to certify that multi-sensor connections work normally for a seismic array even when using a single pair of optical fibers, and 4) to demonstrate effectiveness in preventing signal noise by lightening. The results of the experiments corresponding to aims 1), 2), 3), and 4) are presented in Sections 4, 5.1, 5.2, and 6, respectively.

The layout of the sensor parts, the route of the optical fiber, and the layout of the optical transmitter and receiver devices of the optical interferometry sensor system are shown in **Fig. 3**. We installed an optical transmitter and receiver device, which was attached to a signal processing unit indoors at the HAR, and extended a pair of general-purpose optical fibers from there to connect three sensor parts in series. We refer to the sensor parts as Opt. A, Opt. B, and Opt. C, respectively, in the order of the connections between the optical transmitter and receiver devices. A conventional accelerometer (Hakusan Co., JU210) was installed beside Opt. A for comparison. All three sensors were installed on the ground or on the concrete surface of the ground floor of the building. The sensor parts were placed on the vertices of a triangular shape with sides approximately 40 m to 70 m in length, forming a seismometer array. The horizontal component of the sensor was directed in the N- or E-direction. The positions of the sensor parts Opt. A and Opt. B were estimated from the layouts of the buildings and their relative positions within the buildings (**Fig. 3**). Position of the sensor part Opt. C was estimated from the layout of the GNSS antenna stand and its relative position (**Fig. 3**). The precision of the positions was approximately 0.5 m.

We describe the volcanic activity in Sakurajima during the period when seismic observations using the optical interferometry sensor system were carried out. **Fig. 4** shows the ground deformation and the amount of volcanic ash at Sakurajima from 2007 to 2019. The ground deformation recorded by the extensometers installed in the subsurface observation tunnel located directly below the HAR is shown with two components. The observation period of the optical interferometry sensor system is the period when the trend changes from contraction to extension in the extensometer record. The amount of volcanic ash from Sakurajima was calculated for each month using the

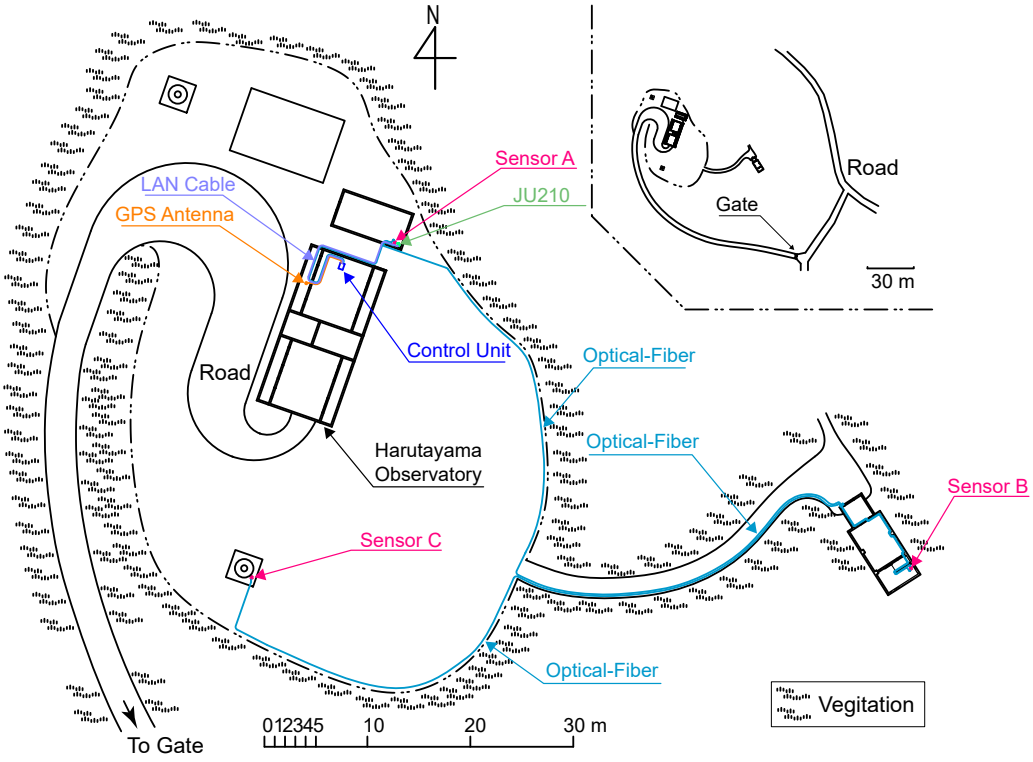

Fig. 3. Layout of the optical interferometry sensor system deployed in the HAR site of Sakurajima Volcano. The light blue line shows the locations where the optical cables are laid.

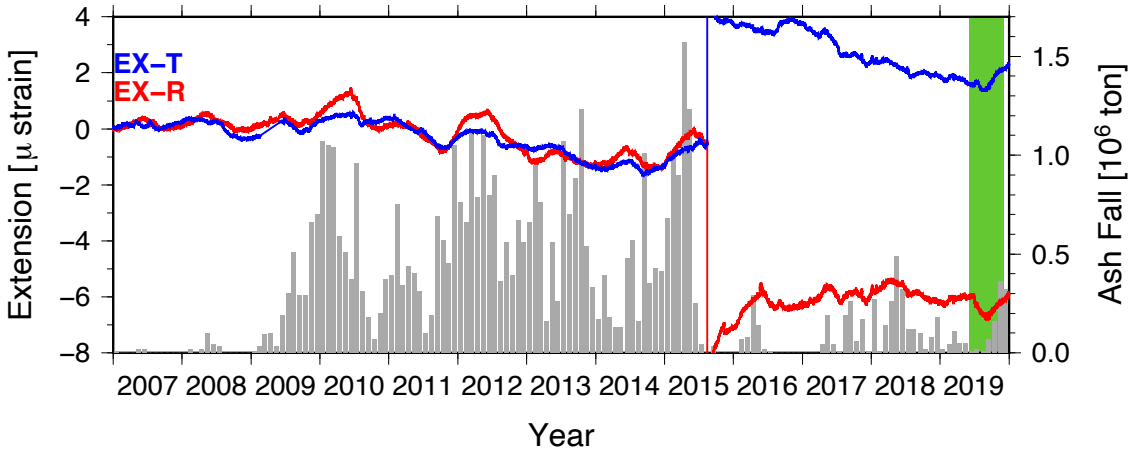

Fig. 4. Volcano ash mass, ground deformation, and observation period from 2007 to 2019 at Sakurajima. Red and blue lines show the records of the extensometer at the observation point HAR. The gray bar shows the volcano ash volume per month. The green frame shows the observation period of the optical interferometry sensor system.

weight of volcanic ash per unit surface area, which was measured by the Kagoshima Prefectural Government at approximately 60 locations in the prefecture [11, 12]. The annual number of volcanic eruptions in 2019 was 393, and the number of volcanic eruptions during the observation period using the optical interferometry sensor system was 260 [13], which means that the seismic observation was carried out at a time when there were relatively many volcanic eruptions.

4. Stability of Data Acquisition and Seismic Waveform

The data were recorded continuously at 200 Hz and 1 kHz in WIN format from 16:00 (JST) on June 5, 2019, to 9:00 on December 5, 2019. In the following analysis, only the 200 Hz sampling data were used. To evaluate the stability of the operation of the system and the effect of natural factors on data recording, we calculated and displayed the number of data files per hour (hourly

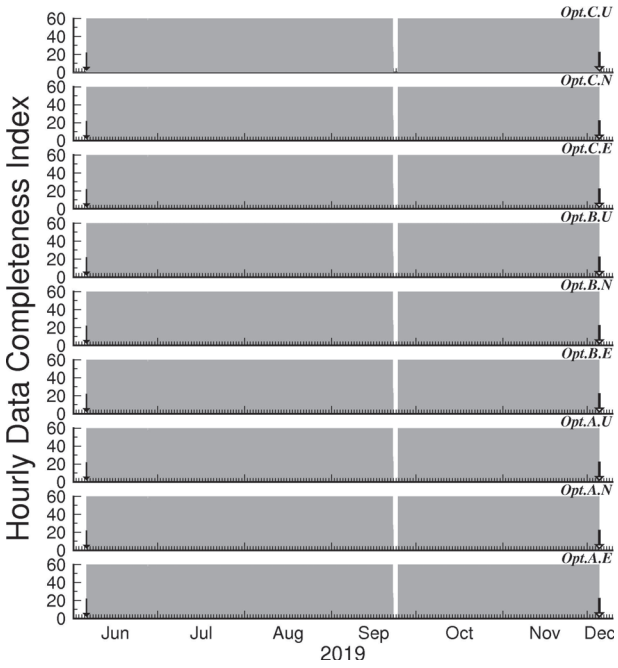

Fig. 5. Acquisition of seismic waveform data by the optical sensor system. Waveform data are recorded into one file per minute, and the hourly data completeness index shows the number of files that are present per hour. This indicates that index value data are present without disruption for every hour.

data completeness index) during the continuous recording period (**Fig. 5**). With the exception of approximately two days in late September 2019, all nine components were observed without missing measurements with an index of 60 consistently from the beginning to the end of recording. Missing measurements occurred from 20:00 (JST) on September 22 to 14:00 on September 24. During this period, several power outages occurred at the HAR, where the system was installed. Because of damage to the power transmission equipment in Sakurajima caused by Typhoon No.17. Power failure occurred several times during this period, and the optical interferometry sensor system repeatedly lost and regained its power. The system was equipped with an uninterruptible power supply (UPS) designed to supply power to the system for 10 minutes for uninterruptible operation. The system is set to shut down automatically during the power outage and reboot automatically soon after the power recovers. However, in reality, the power supply can be interrupted. Finally, the system was restored to operational status at 14:00 on September 24 by an operator who had remotely accessed the system.

Next, we describe the absence of data during the period when digital data were being obtained. Data absence occurs in two cases: software and hardware problems. The software problem occurred on June 23, 2019, after the start of the observation on June 4, 2019. In this case, spiky noise was generated periodically at the end of each second, thereby contaminating the observed data. The spiky noise had an impulsive waveform; however, because it was generated periodically at the end of each second, the noise spectrum had a peak at 1 Hz. This spiky noise is generated by delay correction of the filter process during signal processing. By modifying the filter-processing program on June 23, 2019, the spiky noise disappeared. The hardware problem was found on June 17, 2019, when the signal intensity of the received optical interference was greatly reduced. Therefore, the S/N ratio decreased as the signal intensity decreased. On June 27, 2019, this decrease in the signal intensity of the received optical interference was found to be caused by an abnormal decrease in the gain of the optical amplifier on the optical receiver side, and was addressed by replacing the optical amplifier.

Next, to observe the stability of the observed waveforms, we present an overview of the changes in the seismic amplitude during the entire observation period. Continuous waveform data from Opt. A, Opt. B, and Opt. C of the optical interferometry sensor system and accelerometer JU210 were bandpass-filtered from 0.5 Hz to 20 Hz in order to reduce noise with high and low frequency bands, and resampled at a sampling frequency of 5 Hz. A Hilbert transformation was applied to create envelope waveforms. Finally, the envelope waveforms of the vertical component were resampled at a sampling frequency of 1 Hz to reduce file size, as shown in **Fig. 6**. After the start of the observation at 16:00 on June 5, 2019, the amplitude was large, especially on June 6 and 7, which was caused by the increase in amplitude of the spike-like noise, as mentioned above. There was also a time period from June 25 to June 27 with a large amplitude due to the work to solve the hardware problem described previously. The missing data period from September 22 to September 24 and the timing of the volcanic eruptions during the observation period are also shown in **Fig. 6**. The waveforms of Opt. A of the optical interferometry sensor system and accelerometer JU210 were compared, and it can be seen that they were almost identical except for the data anomaly mentioned above. Comparing Opt. A, Opt. B, and Opt. C, the amplitudes of the three were similar except for the period when the noises, as mentioned above, occurred, and the amplitudes became larger in response to the volcanic eruptions. However, there were timings when volcanic eruptions occurred, but the amplitude was not large, and when no volcanic eruption occurred but the amplitude was large, corresponding to short-lived volcanic eruptions and earthquakes unrelated to volcanic eruptions, respectively. To summarize the above descriptions, observation by the optical interferometry sensor system was generally performed stably during the observation period, excluding problems such as noise and missing data.

5. Results of Analysis

5.1. Waveforms and Spectra of Eruption Events

As mentioned above, 260 earthquakes associated with volcanic eruptions were observed. The sensor part Opt. A of the optical interferometry sensor system and ac-

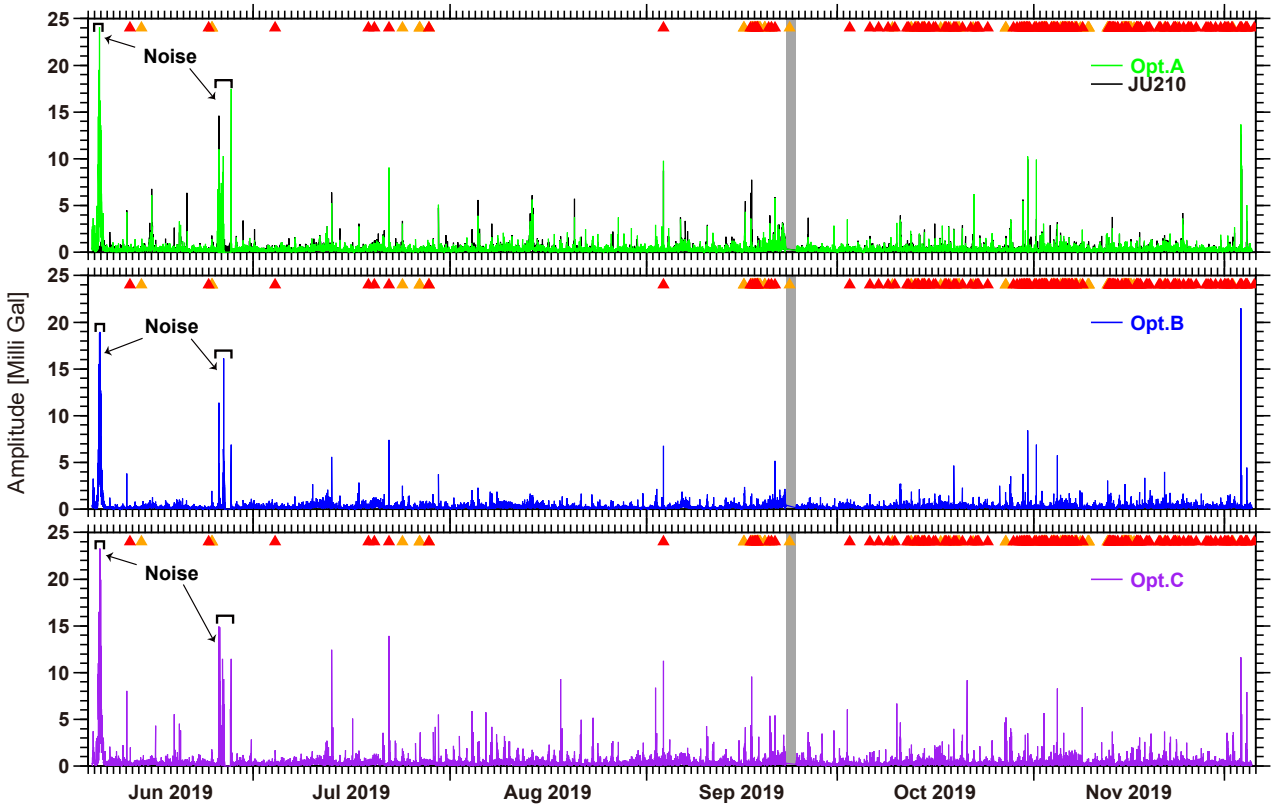

Fig. 6. Envelope waveform for the entire observation period. The vertical gray bar shows the period of missing data (**Fig. 5**). The triangles indicate volcanic eruptions. The red triangles are volcanic eruptions with an amplitude of infrasound of 10 Pa or greater, and the orange triangles are volcanic eruptions with an amplitude of infrasound less than 10 Pa.

celerometer JU210 were compared. A list of earthquakes associated with volcanic eruptions used for comparison is shown in **Table 2**. There were 18 events in **Table 2**, of which the volcanic eruption at 17:24 (JST) on November 8, 2019, which had the highest eruption column during the observation period, and the volcanic eruption at 17:33 on November 18, 2019, which had the largest infrasound amplitude during the observation period, are shown in **Figs. 7** and **8**, respectively. Opt. A and JU210, installed at site A (**Fig. 3**), are both accelerometers. By integrating the waveforms from Opt. A and JU210, the velocity waveforms are obtained, as shown in typical seismograms for volcanic earthquakes. For Opt. A and JU210, no correction of the seismometer frequency response was made to the seismic records. A time window of 80 s was used to extract the seismic waveform associated with volcanic eruption to cover the whole seismogram from the P-wave arrival to the coda wave, and the power spectral density of the velocity was calculated by performing a fast Fourier transform on the extracted waveform with Hamming window after removing an offset and a linear trend of the waveform.

Figures 7 and **8** show seismograms of JU210 (blue) and Opt. A (red) from top to bottom, and their spectra are presented in the same colors. As shown in **Figs. 7** and **8**, the waveforms and spectra are generally identical. However, the spectra show a difference in the low-frequency range of 0.2 Hz to 0.5 Hz, and Opt. A often exhibits a

Table 2. List of eruptions.

Day time yyyy-mm-ddThh:mm	Plume height [m]	Air maximum amplitude [Pa]	Figure number
2019-07-24T13:09	1500	15.6	–
2019-09-17T09:27	1000	90.1	–
2019-09-18T10:47	2600	61.8	–
2019-10-12T06:36	1400	19.7	–
2019-10-13T17:28	700	25.4	–
2019-10-13T20:59	300	84.2	–
2019-10-29T09:35	1500	26.4	–
2019-10-30T09:07	1200	8.1	–
2019-11-03T01:46	1600	28.5	–
2019-11-07T02:36	2600	39.9	–
2019-11-08T17:24	5500	36.6	7
2019-11-12T20:20	3300	10.9	–
2019-11-17T05:28	1500	35.3	–
2019-11-17T13:51	2200	68.8	–
2019-11-18T17:33	1500	144.1	8
2019-11-23T00:42	1800	37.1	–
2019-11-28T21:30	2600	20.5	–
2019-12-02T06:22	1500	18.6	–

This list was extracted from the Kagoshima Meteorological Office [13]. The maximum amplitude of the infrasound waves associated with eruptions was obtained from the maximum value between the stations measured by the Kagoshima Meteorological Office.

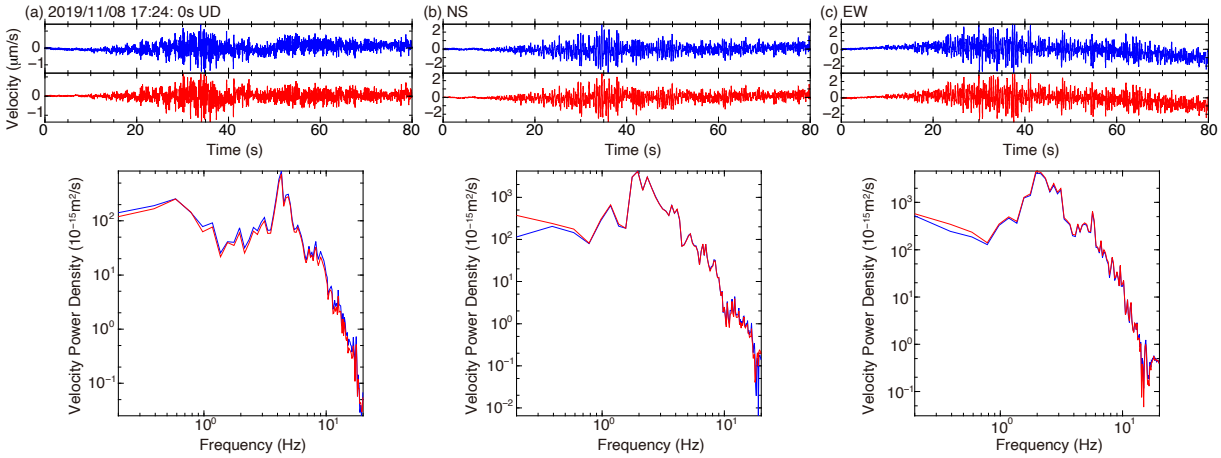

Fig. 7. Seismogram and corresponding power spectral density associated with volcanic eruption at 17:24 on November 6, 2019. The frequency range of the spectral density displayed is 0.2–20 Hz. (a) Vertical component, (b) north-south component, and (c) east-west component. The line color corresponds to the type of the seismometer: the blue line indicates the JU210 accelerometer and the red line Opt. A of the optical interferometry sensor system.

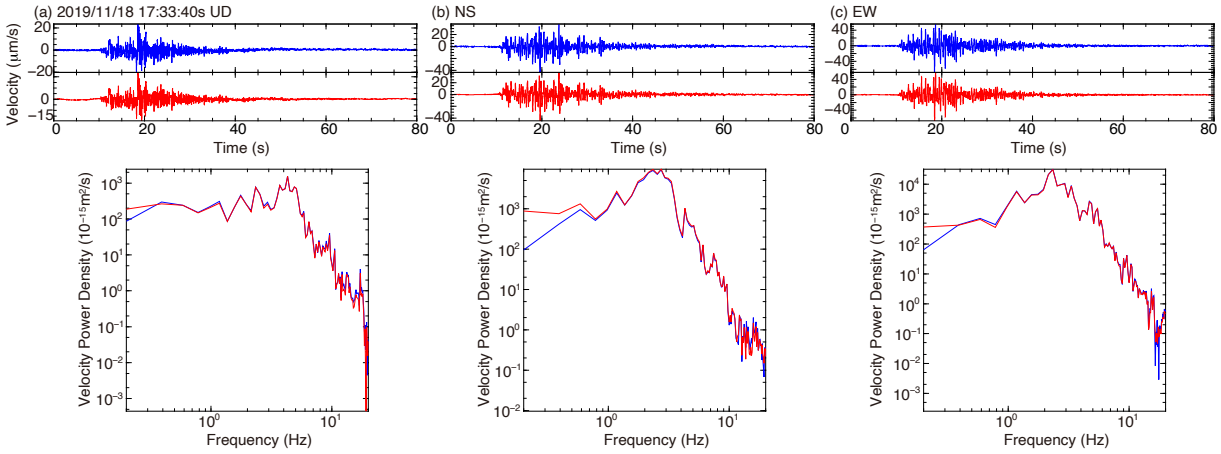

Fig. 8. Earthquake record and corresponding power spectral density associated with volcanic eruption at 17:33 on November 18, 2019. Graphical details are the same as in **Fig. 7**.

larger amplitude than JU210. We estimate that the larger amplitude in the low-frequency range is due to the high noise level caused by the temperature fluctuations and not true seismic ground motion. The causes of noise in the low-frequency range have not been quantitatively evaluated; therefore, the causes of noise are described qualitatively. From previous observations [10], it is known that noise in the low-frequency range exists regardless of the environment in which the sensor is installed. It has also been found that when the temperature at the location where the optical transmitter and receiver devices are installed suddenly changes, the amplitude of the noise changes. Therefore, the temperature change in the optical device may affect optical pulse interferometry. Because the wavelength of the optical pulse fluctuates with the temperature change, it is estimated that the cause of the noise is a phase change due to the fluctuation of the wavelength generated when the optical device interferes with the light and the signal processing unit performs arithmetic processing. Because the optical device has a function to stabilize the wavelength of the optical pulse and the wavelength is continuously adjusted in time, the noise in the acceleration output from the signal processing unit is considered more remarkable in the low-frequency range such as 0.2 Hz to 0.5 Hz than at higher frequencies.

5.2. Array Analysis of Eruption Events

As mentioned earlier, the sensor parts (seismometers) of the optical interferometry sensor system are arranged at the vertices of a triangular shape, forming a seismometer array (**Fig. 3**), which enables the array analysis of seismic waves. However, it is important to evaluate the accuracy of the estimation of the arrival direction and slowness of seismic waves for array analysis because our minimum array configuration has only three sensor sites. Therefore, we first evaluated the directional sensitivity and resolution power of the array, as described by the beam-forming array response at 2.5 Hz, which is the frequency with suffi-

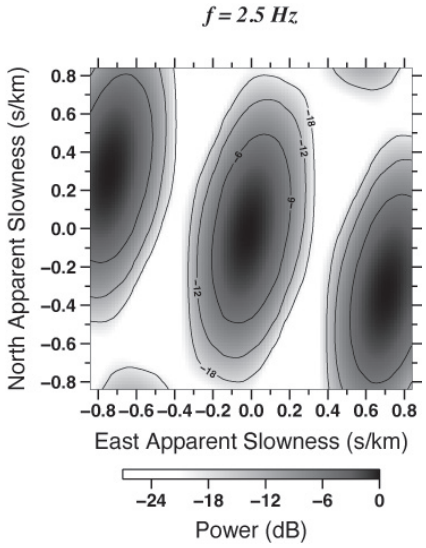

Fig. 9. Beam-forming array response at 2.5 Hz for east and north components of the slowness from −0.84 s/km to 0.84 s/km.

cient seismic energies associated with volcanic eruptions (**Figs. 7** and **8**). **Fig. 9** shows that the side lobes in the response are broadened in the north-south direction, indicating that this array cannot constrain the slowness of the waves in the north-south direction.

We used the semblance technique [14] to measure the apparent slowness and back azimuth of the coherent wave phases that crossed the array. We calculated the semblance values for the selected array data at all the apparent slowness and back-azimuth grid nodes. The position of the nodes with the maximum semblance value provides an estimate of the apparent slowness and back azimuth of the incoming wavefronts. Semblance analysis of the vertical components of the seismograms was performed. After filtering the waveform data at 2–3 Hz, the semblance coefficient was calculated for a time window of 1 s. We performed this analysis in which the time window started from the beginning of the selected waveform of 80 s length, which includes the whole signal of a volcanic eruption (**Figs. 7** and **8**), and moved successively by 0.1 s until the end of the waveform. We adopted the time shift length to reduce the necessary computation time and obtain sufficient time resolution for the wave propagation parameters. The range of apparent slowness was searched from 0.01 s/km to 3.20 s/km in steps of 0.01 s/km, and the range of back azimuth was searched from 0° to 355° (measured clockwise from north) in 1° steps in this analysis.

Figure 10 shows an example of the array analysis results. The earthquake occurred at 17:33 (JST) on November 18, 2019, and was one of the earthquakes whose waveform and spectrum are shown in **Fig. 8**. **Fig. 10** shows, from top to bottom, the filtered waveform, the semblance value slowness, and the back azimuth (opposite direction of the traveling wave) for each analysis window. The results for each time window are shown in the range of 0.0 s/km to 1.5 s/km for the slowness and 30° to 210° for the back azimuth. The slowness maps for time windows A, B, and C are shown in the vertical red belts at the bottom of the figure. Time window A corresponds to the first motion of the earthquake. In time window A and the 10 time windows behind it, the semblance value is 0.98, the slowness is 0.34 s/km, and the back azimuth is distributed from 129° to 139° from north to east, which is significantly shifted from the direction of the array to the direction of Minamidake Crater in the counterclockwise direction. The slowness map for time window A shows that the region with a semblance value of 0.9 or higher is an ellipse with a longer axis in the north-south direction. Therefore, we can conclude that the uncertainty of the back azimuth is large. The fact that the spread in the east-west direction is narrower than that in the north-south direction is supported by the fact that the slowness is stable at a constant value. The characteristics of this semblance slowness map can be explained by the array response shown in **Fig. 9**. In time window B, the slowness was as small as 0.15 s/km, and the back azimuth was 47° from north to east. This wave does not come from Minamidake Crater but is likely to be a reflected wave in the crust coming from the subsurface of northern Sakurajima. However, as can be seen from the semblance slowness map of time window B, it is difficult to estimate the reflection point because the region with a semblance value of 0.9 or higher extends from north to south. In time window C, the slowness is 0.38 s/km and the back azimuth is 115°. Considering the distribution of semblance values of 0.9 or more in the semblance slowness map in time window C, the wave in time window C is a coherent wave coming from the crater, and if time window A corresponds to the start of the first eruption, time window C might correspond to the start of the second eruption.

Figure 11 shows the results of the array analysis of the P-wave initial motion (corresponding to time window A in **Fig. 10**) for earthquakes caused by 194 volcanic eruptions that were observed with a sufficient S/N ratio among the 260 eruptions that occurred during the observation period. The volcanic eruptions listed in **Table 2** are among the 194 eruptions. **Fig. 11(a)** shows the frequency distribution of the back azimuth in a rose diagram, and **Fig. 11(b)** shows the frequency distribution of slowness. The most frequent back azimuth is in the range of 135° to 140°, which is approximately 40% of the total number of volcanic eruptions. The most frequent slowness is in the rage of 0.30 s/km to 0.35 s/km, which is 46% of the total number of volcanic eruptions. This slowness range includes 0.34 s/km, which is the result of the analysis, as shown in **Fig. 10**. The distributions of the back-azimuth frequency and slowness frequency vary with a peak, as shown in **Figs. 11(a)** and **(b)**, respectively. However, one can consider that these variations can be attributed to the array response. As a result, the source locations of the earthquakes associated with the volcanic eruptions were considered stable and did not change significantly from one volcanic eruption to another. The slowness of 0.34 s/km of the initial P-wave motion, as shown in **Fig. 10**, is almost

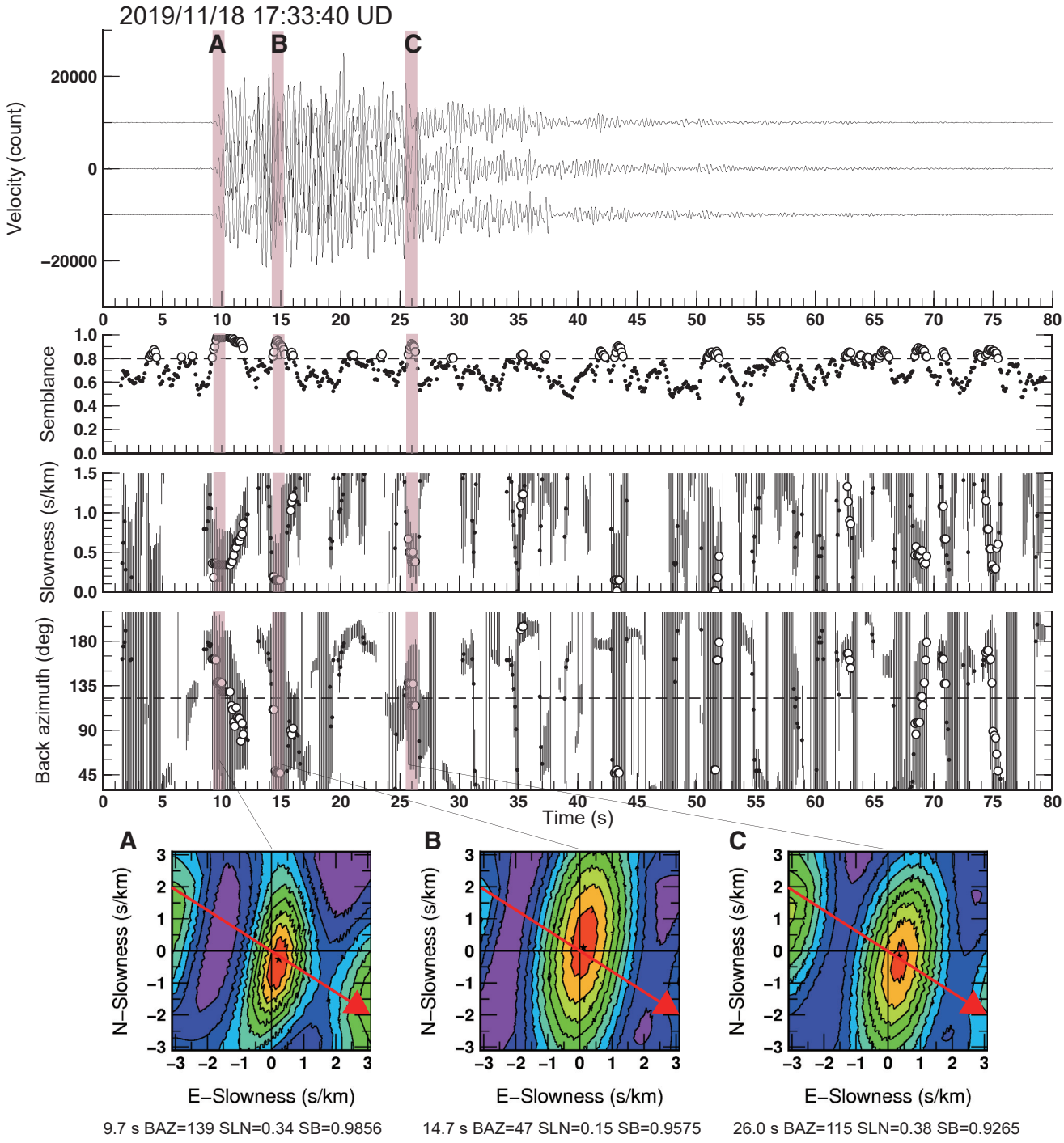

Fig. 10. Results of array analysis of earthquakes associated with volcanic eruption. Waveforms from three seismometers (2–3 Hz bandpass filter), semblance, slowness, back azimuth, and semblance-slowness map are shown from top to bottom. The horizontal dashed line on the back-azimuth diagram shows the direction of Minamidake Crater (N123°E) from the array. The color of the semblance-slowness map indicates values from 0.0 to 1.0 in increments of 0.1, with the red color showing 0.9 to 1.0 and purple color showing 0.0 to 0.1. The red arrow points in the direction of Minamidake Crater.

equal to the slowness of 0.37 s/km obtained from the apparent P-wave velocity of 2.7 km/s of the earthquake associated with the Minamidake eruption on September 4, 1999 [15]. Assuming the 1D (one-dimensional) velocity structure assumed in the seismic reflection survey [16] and the epicenter to be Minamidake Crater, we can explain the slowness of 0.34 s/km at a source depth of 1.6 km below sea level. This depth is almost the same as that estimated from the moment tensor analysis of earthquakes associated with volcanic eruptions in Minamidake Crater, 1.8 km to 2.2 km [15]. Therefore, it is demonstrated that the optical interferometry system produced data useful for the analysis of earthquakes associated with volcanic eruptions, although the number of sensor parts

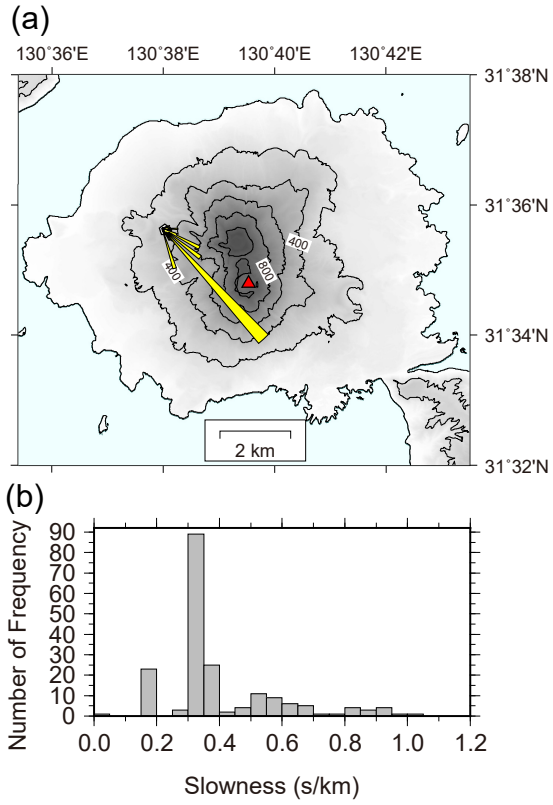

Fig. 11. (a) Rose diagram in 5° increments. The direction of the most frequent value of back azimuth is in the range of 135° to 140°, and the frequency in this direction is 75. (b) The frequency of slowness is displayed in increments of 0.05 s/km. The maximum frequency of slowness is in the range of 0.3 s/km to 0.35 s/km, and the frequency in this range is 89.

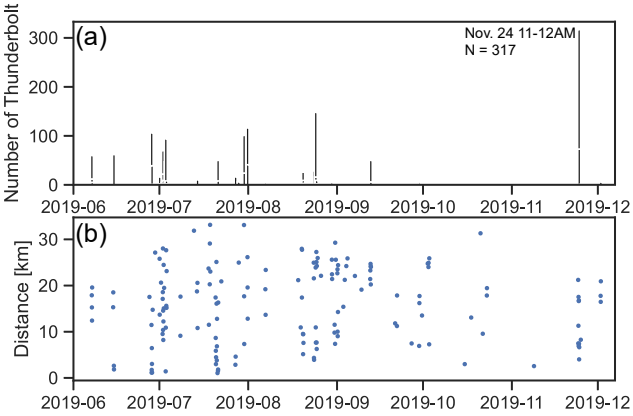

Fig. 12. Lightning activity around Sakurajima. (a) Frequency of lightning strikes per hour. (b) Distance from HAR to the lightning strike point.

(seismometers) of the system was as small as three. The optical interferometry system successfully realized a seismic array using even a single couple of optical fibers with three sensors. This suggests that the system has the potential to support larger-scale arrays with more nodes using even a single couple of optical fibers in volcanoes, as well as other geologic sites.

6. Waveforms and Spectra During Which Lightning Occurs

We investigated the performance of lightning resistance in seismic observations using an optical interferometry sensor system deployed in Sakurajima for six months starting in June 2019. First, a survey of lightning occurrences during the observation period was conducted, with the HAR as the center point and an area of 50 km × 50 km extending in the north-south and east-west directions as the survey area. The distance to electrical equipment affected by lightning surges was approximately 2 km [17]. In this case, it was difficult to locate the falling positions of the lightning within a distance of 2 km; therefore, the search area was much wider than the distance for investigating the lightning occurrence. The presence/absence of lightning storms, number of lightning storms, and shortest distance from the center point for each time period during the survey period are shown in **Fig. 12**. The rainy season of 2019 began on May 31 and ended on July 24 in southern Kyushu, where Sakurajima is located. The number of lightning strikes was high in June and July during the rainy season (**Fig. 12(a)**). Outside the rainy season, the number of lightning strikes was high in late August and on November 24. In particular, on November 24, 317 lightning strikes occurred between 11:00 and 12:00, and the shortest distance was 4.0 km (**Fig. 12(b)**). The seismic waveform recorded during this period is shown in **Fig. 13**. During this period, volcanic eruptions, volcano tectonic earthquakes, and tectonic earthquakes did not occur. On the other hand, low-frequency earthquakes and volcanic tremors occurred and were observed by both the optical interferometry sensor system and accelerometer JU210, as shown by the hatches in **Fig. 13**. By comparing the waveforms of the optical interferometry sensor system, Opt. A, and accelerometer JU210 installed in the same location, a pulse-like wave with a short duration (red reversed triangles and inset in **Fig. 13**) can be seen in the seismic record of JU210, although it cannot be seen in the seismic record of the optical interferometry sensor system. This is thought to be due to electrical noise (lightning surges) from lightning strikes.

The running spectrum was calculated to evaluate the effect of lightning surge on earthquake observations in more detail. For the period 11:00–12:00 on November 24, as shown in **Fig. 14(a)**, the power spectrum densities of the acceleration in the vertical motion component record of the optical interferometry sensor system, Opt. A, and the accelerometer JU210 installed at the same location are shown in **Fig. 14(b)**. We can see that there is power in the broad frequency band for JU210 at eight times that correspond to the arrival times of the pulsed waves (arrows in **Fig. 14(b)**). However, the power in the broad frequency band at these times that JU210 could recognize is not found in the spectrum of Opt. A. As mentioned above,

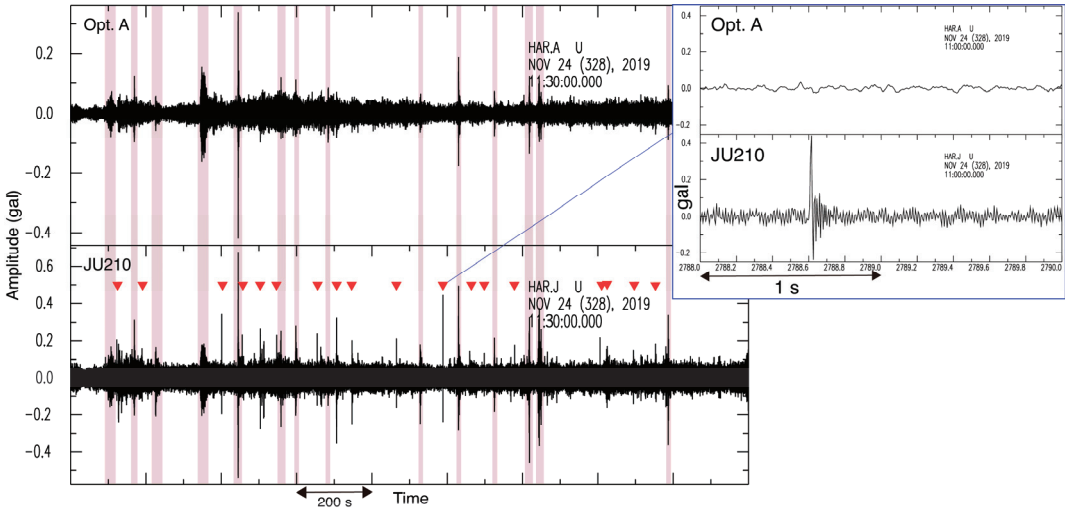

Fig. 13. Seismic waveform records of the UD component of Opt. A (top) and JU210 (bottom) at the time of most frequent lightning strikes (11:30–12:00 on November 24, 2019). The hatching shows times when a volcanic tremor or a low-frequency earthquake occurred. The red reversed triangles show the time when the lightning was supposed to have affected the data recorded for JU210. The inset shows the 2-second waveforms of Opt. A (top) and JU210 (bottom) during the time when pulsed noise is mixed in JU210.

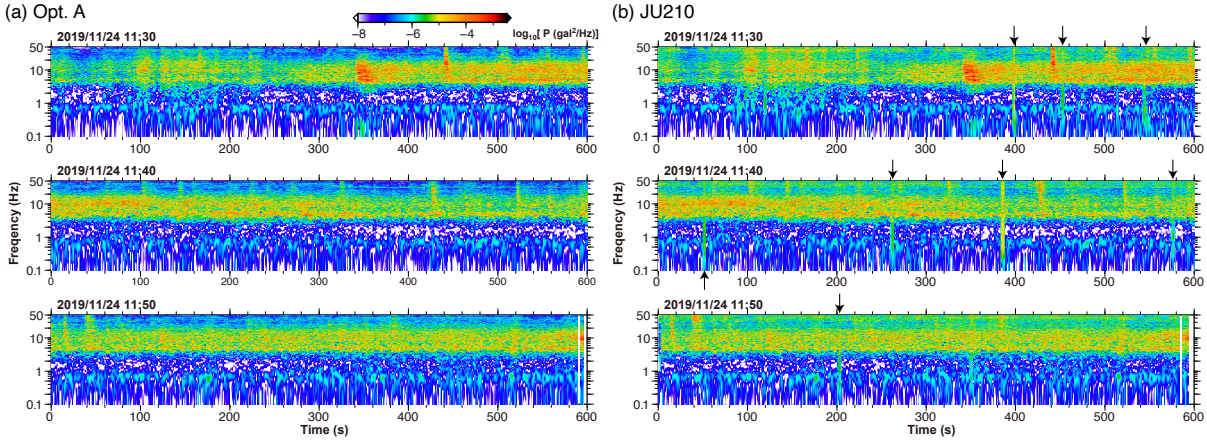

Fig. 14. Running spectrum at the time of most frequent lightning strikes (11:00–12:00 on November 24, 2019). The power spectrum density of the acceleration of the vertical motion component is shown in the color scale. (a) Optical interferometry sensor system Opt. A. (b) Accelerometer JU210.

JU210 had a pulse-like noise waveform at the corresponding times, and the spectrum had broadband power. In the running spectrum of JU210, the power was continuously observed at approximately 40 Hz, whereas it was not observed in the running spectrum of Opt. A. The power near 40 Hz is almost proportional to the power in the other frequency bands. Therefore, the presence or absence of power near 40 Hz is considered to reflect the difference in the noise level in frequency in the data recorded from the seismometers of Opt. A, and JU210 [18]. It was shown above that the optical interferometry sensor system and the existing accelerometers can observe low-frequency earthquakes and volcanic tremors, and are not affected by the noise caused by the lightning surge, except for the difference in frequencies at 40 Hz.

To evaluate in further detail the effect of the lightning surge of the optical interferometry system, we calculated the root-mean-square (RMS) amplitudes in the time window of 0.1 s of the pulse-like waves of the vertical component of JU210 and the RMS amplitudes of the vertical component of Opt. A in the same time window as for JU210. **Fig. 15(a)** shows a histogram of the RMS amplitude for Opt. A and JU210 of the 44 pulse-like waves. While the RMS amplitudes of JU210 are distributed in the range from 0.03 gal to 0.2 gal, the amplitudes of Opt. A are distributed in the range from 0 gal to 0.3 gal. The ratio of the RMS amplitudes for Opt. A to those for JU210 is less than 0.2 (**Fig. 15(b)**), demonstrating that Opt. A shows a much smaller effect from the lightning surge in the records. Therefore, it can be considered that the optical interferometry sensor system is an effective seismic observation tool in fields affected by lightning, such as volcano zones.

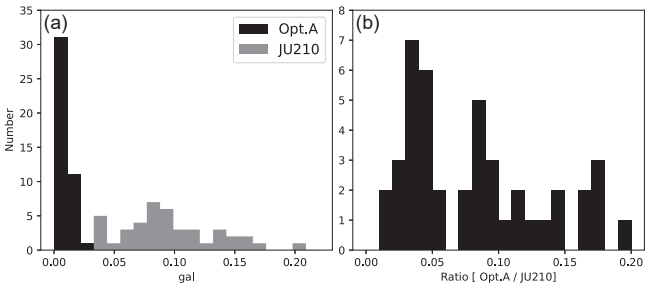

Fig. 15. (a) Histograms of the root-mean-square (RMS) amplitudes of the pulse-like waves of the vertical component of JU210 and the RMS amplitudes of the vertical component of Opt. A in the same time window. (b) Histogram of the RMS amplitude ratio of Opt. A to JU210.

7. Summary

Continuous seismic observations for approximately six months from June to December 2019 were carried out using an optical interferometry sensor system, including the period of lightning strikes at Sakurajima Volcano, which has the highest volcanic eruption rate in Japan. The observations were stopped for a few days due to power failure, but otherwise continuous operation was successfully carried out. During the observation period, 260 volcanic eruptions were observed. The observation performance of the optical interferometry sensor system was evaluated for earthquakes associated with volcanic eruptions by spectral analysis and array analysis, and it was confirmed that the performance was sufficient for the analysis of these earthquakes. By comparing the waveforms and spectra of the optical interferometry sensor system with those of an accelerometer during lightning strikes, it was shown that pulse-like noise caused by lightning surges was observed in the accelerometer, but not in the optical interferometry sensor system. This indicates that the optical interferometry sensor system can perform seismic observations without being affected by lightning strikes. Although the optical interferometry sensor system has some observational limitations because it requires a commercial power source, it is possible to carry out seismic observations flexibly by laying seismometers and optical fibers; thus, a seismic observation network can be deployed near the top of the volcanoes. In addition, it exhibits sufficient performance and lightning resistance to reliably observe volcanic seismic events; therefore, it is an effective method for monitoring volcanic activity.

Acknowledgments

This work was based on the B2-2 project titled "Development of multi-channeled seismometer system with phase-shifted optical interferometry for volcanological observations" as a part of the Integrated Program for Next Generation Volcano Research and Human Resource Development Project Grant Number JPJ005391 founded by Japan Ministry of Education, Culture, Sports, Science and Technology (MEXT). We are very grateful to all staff of the Sakurajima Volcano Research Center, Disaster Pretension Research Institute, Kyoto University, for field deployment in the HAR at Sakurajima. Special thanks to Prof. Tomoki Tsutsui for advising us on the project. We are grateful to the reviewers and the editor for their constructive comments and suggestions.

References:

[1] K. Hamada, M. Ohtake, Y. Okada et al., "Kanto-Tokai Observation Network of Crustal Activities-National Research Center for Disaster Prevention," Zisin, Vol.35, No.3, pp. 401-426, doi: 10.4294/zisin1948.35.3_401, 1982 (in Japanese).

[2] Y. Okada, "Seismology: First results from Japanese network for earthquake prediction," Nature, Vol.312, No.5994, pp. 500-501, doi: 10.1038/312500a0, 1984.

[3] Y. Okada, K. Kasahara, S. Hori et al., "Recent progress of seismic observation networks in Japan – Hi-net, F-net, K-NET and KiK-net –," Earth, Planets and Space, Vol.56, No.8, pp. xv-xxviii, doi: 10.1186/BF03353076, 2004.

[4] K. Obara, K. Kasahara, S. Hori et al., "A densely distributed high-sensitivity seismograph network in Japan: Hi-net by National Research Institute for Earth Science and Disaster Prevention," Rev. Sci. Instrum., Vol.76, No.2, Article No.021031, doi: 10.1063/1.1854197, 2005.

[5] T. Tanada, H. Ueda, M. Nagai et al., "NIED's V-net, the fundamental volcano observation network in Japan," J. Disaster Res., Vol.12, No.5, pp. 926-931, doi: 10.20965/jdr.2017.p0926, 2017.

[6] Z. Zhan, "Distributed acoustic sensing turns fiber-optic cables into sensitive seismic antennas," Seismol. Res. Lett., Vol.91, No.1, pp. 1-15, doi: 10.1785/0220190112, 2019.

[7] T. Nishimura, K. Emoto, H. Nakahara et al., "Source location of volcanic earthquake and subsurface characterization using fiber-optic cable and distributed acoustic sensing system," Sci. Rep., Vol.11, Article No.6319, doi: 10.1038/s41598-021-85621-8, 2021.

[8] M. Yoshida, Y. Hirayama, A. Takahara et al., "Real-time displacement measurement system using phase-shifted optical pulse interferometry: Application to a seismic observation system," Jpn. J. Appl. Phys., Vol.55, No.2, Article No.022701, doi: 10.7567/JJAP.55.022701, 2016.

[9] Y. Ohe, H. Kimura, N. Inou et al., "Verification of principle of a new vibrating sensor with optical interferometry and the application possibility," Trans. Soc. Instrum. Control Eng., Vol.54, No.1, pp. 111-117, 2018 (in Japanese).

[10] T. Tsutsui, Y. Hirayama, T. Ikeda et al., "Feasibility study on a multi-channeled seismometer system with phase-shifted optical interferometry for volcanological observations," J. Disaster Res., Vol.14, No.4, pp. 592-603, doi: 10.20965/jdr.2019.p0592, 2019.

[11] T. Eto, "An estimation of the amount and the dispersal of volcanic ash-falls ejected by summit eruptions at Sakurajima Volcano," Proc. Kagoshima Int. Conf. on Volcanoes, pp. 448-451, 1989.

[12] T. Eto, "Estimation of the amount and dispersal of volcanic ash-fall deposits ejected by vulcanian type eruption," Rep. Fac. Sci. Kagoshima Univ., Vol.34, pp. 35-46, 2001.

[13] Kagoshima Meteorological Office, https://www.jma-net.go.jp/kagoshima/vol/data/skr_exp_list/skr_exp_2019.html [accessed May 6, 2022]

[14] N. S. Neidell and M. T. Taner, "Semblance and other coherency measures for multichannel data," Geophysics, Vol.36, No.3, pp. 482-497, doi: 10.1190/1.1440186, 1971.

[15] T. Tameguri, M. Iguchi, and K. Ishihara, "Mechanism of explosive eruptions from moment tensor analyses of explosion earthquakes at Sakurajima Volcano, Japan," Bull. Volcanol. Soc. Japan, Vol.47, No.4, pp. 197-215, doi: 10.18940/kazan.47.4_197, 2002.

[16] T. Tsutsui, M. Iguchi, T. Tameguri et al., "Structural evolution beneath Sakurajima Volcano, Japan, revealed through rounds of controlled seismic experiments," J. Volcanol. Geotherm. Res., Vol.315, pp. 1-14, doi: 10.1016/j.jvolgeores.2016.02.008, 2016.

[17] R. H. Golde, "Lightning surges on overhead distribution lines caused by indirect and direct lightning strokes [includes discussion]," Trans. American Inst. Electrical Engineers Part III: Power Apparatus and Systems, Vol.73, Issue 1, pp. 437-447, doi: 10.1109/AIEEPAS.1954.4498839, 1954.

[18] Hakusan Corporation, https://www.hakusan.co.jp/english/solution/optical_sensor [accessed May 6, 2022]

Name:
Haruhisa Nakamichi

Affiliation:
Associate Professor, Sakurajima Volcano Research Center, Disaster Prevention Research Institute (DPRI), Kyoto University

Address:
1722-19 Sakurajima-Yokoyama-cho, Kagoshima 891-1419, Japan

Brief Career:
2003-2005 JSPS Research Fellow, National Research Institute for Earth Science and Disaster Prevention
2005-2013 Assistant Professor, Graduate School of Environmental Studies, Nagoya University
2013- DPRI, Kyoto University

Selected Publications:
• "Dike inflation process beneath Sakurajima Volcano, Japan, during the earthquake swarm of August 15, 2015," Frontiers in Earth Science, Vol.8, Article No.600223, doi: 10.3389/feart.2020.600223, 2021.
• "A newly installed seismic and geodetic observational system at five Indonesian volcanoes as part of the SATREPS project," J. Disaster Res., Vol.14, No.1, pp. 6-17, doi: 10.20965/jdr.2019.p0006, 2019.
• "Differences of precursory seismic energy release for the 2007 effusive dome-forming and 2014 Plinian eruptions at Kelud Volcano, Indonesia," J. of Volcanology and Geothermal Research, Vol.382, pp. 68-80, doi: 10.1016/j.jvolgeores.2017.08.004, 2019.

Academic Societies & Scientific Organizations:
• Volcanological Society of Japan (VSJ)
• Japan Geoscience Union (JpGU)
• International Association of Volcanology and Chemistry of the Earth's Interior (IAVCEI)
• American Geophysical Union (AGU)

Name:
Yoshiharu Hirayama

Affiliation:
Manager, Research & Development Department, Hakusan Corporation

Address:
J Tower, 1-1 Nikko-cho, Fuchu, Tokyo 183-0044, Japan

Brief Career:
1996- Hakusan Corporation

Selected Publications:
• "Real-time displacement measurement system using phase-shifted optical pulse interferometry: Application to a seismic observation system," Jpn. J. Appl. Phys., Vol.55, No.2, Article No.022701, doi: 10.7567/JJAP.55.022701, 2016.

Academic Societies & Scientific Organizations:
• Volcanological Society of Japan (VSJ)
• Seismological Society of Japan (SSJ)

Name:
Toshiharu Ikeda

Affiliation:
Associate Senior Manager, Research & Development Department, Hakusan Corporation

Address:
J Tower, 1-1 Nikko-cho, Fuchu, Tokyo 183-0044, Japan

Brief Career:
2010- Hakusan Corporation

Selected Publications:
• "Real-time displacement measurement system using phase-shifted optical pulse interferometry: Application to a seismic observation system," Jpn. J. Appl. Phys., Vol.55, No.2, Article No.022701, doi: 10.7567/JJAP.55.022701, 2016.

Name:
Hiroshi Ando

Affiliation:
Technical Manager, Disaster Risk Management Division, Hakusan Corporation

Address:
J Tower, 1-1 Nikko-cho, Fuchu, Tokyo 183-0044, Japan

Brief Career:
1995- Hakusan Corporation

Selected Publications:
• "Feasibility study on a multi-channeled seismometer system with phase-shifted optical interferometry for volcanological observations," J. Disaster Res., Vol.14, No.4, pp. 592-603, doi: 10.20965/jdr.2019.p0592, 2019.

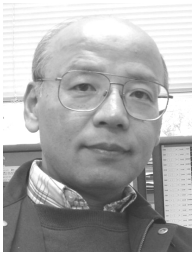

Name:
Keiji Takeuchi

Affiliation:
Chief Engineer, Research & Development Department, Hakusan Corporation

Address:
J Tower, 1-1 Nikko-cho, Fuchu, Tokyo 183-0044, Japan

Brief Career:
1978-1997 Japan Weather Association
1997- Hakusan Corporation

Selected Publications:
• "Real-time displacement measurement system using phase-shifted optical pulse interferometry: Application to a seismic observation system," Jpn. J. Appl. Phys., Vol.55, No.2, Article No.022701, doi: 10.7567/JJAP.55.022701, 2016.